

# Electrochemically induced carbon dioxide capture from air with an aqueous fluoflavine sorbent

Zhuwen Wei<sup>†1</sup>, Sheng Xu<sup>†1</sup>, Jinxin Liu<sup>2</sup>, Kaiping Zhu<sup>1</sup>, Mengke Tang<sup>3</sup>, Aini Li<sup>1</sup>, Xingqi Wang<sup>1</sup>, Kean Ping (Leah) Tan<sup>4</sup>, Yang Li<sup>3✉</sup>, Zheng Meng<sup>2✉</sup>, Yan Jing<sup>1✉</sup>

<sup>1</sup>Department of Materials Science and Engineering, National University of Singapore, 117576, Singapore.

<sup>2</sup> State Key Laboratory of Precision and Intelligent Chemistry, Department of Chemistry, University of Science and Technology of China, Hefei, Anhui 230026, P. R. China.

<sup>3</sup> State Key Laboratory of Information Photonic and Optical Communications, and School of Science, Beijing University of Posts and Telecommunications, Beijing 100876, P. R. China.

<sup>4</sup> Department of Mechanical Engineering, National University of Singapore, 117583, Singapore.

<sup>†</sup>These authors contributed equally to this work.

✉ e-mail: [liyang1988@bupt.edu.cn](mailto:liyang1988@bupt.edu.cn); [zhengmeng@ustc.edu.cn](mailto:zhengmeng@ustc.edu.cn); [yan-jing@nus.edu.sg](mailto:yan-jing@nus.edu.sg).

## Abstract

Direct air capture (DAC) holds great potential in mitigating climate change. A promising approach is redox sorbent-based electrochemically induced DAC, which operates at ambient conditions with significantly lower energy costs while utilizing clean electricity. However, the oxygen sensitivity of redox sorbents remains a major challenge. Thus, the feasibility of achieving electrochemically induced DAC with redox sorbents remains uncertain. Despite the vast difference in partial pressures between carbon dioxide ( $\text{CO}_2$ ) and molecular oxygen ( $\text{O}_2$ ) in air, ribulose-1,5-bisphosphate in plant leaves can preferentially react with  $\text{CO}_2$  in the sunlight, thus achieving the net  $\text{CO}_2$  removal. Motivated by the nature-based DAC solution, we hereby developed an aqueous-soluble oxygen-tolerant fluoflavine disulfonate (**FFDS**) sorbent for DAC. Electrochemical characterizations, spectroscopic studies, along with theoretical calculations, reveal that **FFDS** undergoes proton-coupled electron transfer and exhibits a redox potential higher than the two-electron transfer oxygen reduction potential. When exposed to simulated flue gas containing 10%  $\text{O}_2$ , the **FFDS** sorbent demonstrates reversible  $\text{CO}_2$  capture and release with an average  $\text{CO}_2/e$  molar ratio of 0.88. Implemented for both indoor and outdoor DAC in Singapore, **FFDS** sorbent shows stable cycling performance over 40 days with a three-day DAC under the normal discharge–charge mode, and exhibits an enhanced  $\text{CO}_2$  capture capacity and a Coulombic efficiency exceeding 99% with an accelerated overnight DAC under the deep discharge–charge mode. Doubling the concentration of **FFDS** leads to a twofold increase in  $\text{CO}_2$  capture/release capacity, regardless of whether the three-day DAC is conducted indoors or outdoors. The energy cost for  $\text{CO}_2$  release and sorbent regeneration ranges from 58 to 190  $\text{kJ mol}^{-1}$   $\text{CO}_2$ , depending on the applied current densities and discharge–charge modes.

## Introduction

Capturing carbon dioxide ( $\text{CO}_2$ ) from point or diffuse sources is urgently needed to mitigate climate change. Existing technologies, including amine scrubbing for point source capture<sup>[1]</sup> and hydroxide-based solutions<sup>[2]</sup> for direct air capture (DAC), rely on temperature-swing and require high energy input for sorbent regeneration and  $\text{CO}_2$  release.

Potentially operating entirely on clean electricity, electrochemically induced  $\text{CO}_2$  capture approach using redox sorbents offers a promising alternative to thermochemical methods, as the process enables reversible  $\text{CO}_2$  release and sorbent regeneration under isothermal conditions by alternating electrochemical potentials, significantly lowering energy costs.<sup>[3–9]</sup>

A number of electrochemically redox-active sorbents have been investigated in both aqueous<sup>[5, 6, 10–16]</sup> and nonaqueous<sup>[3, 17–25]</sup> media for reversible  $\text{CO}_2$  capture and release through nucleophilicity-swing and/or pH-swing. Despite the promise of low energy cost and operating at ambient conditions, a key challenge remains: the poor selectivity of sorbents for  $\text{CO}_2$  over molecular oxygen ( $\text{O}_2$ ).<sup>[15]</sup> This issue arises because, after sorbent regeneration, the electrochemically reduced species are more likely to be

re-oxidized by O<sub>2</sub>, rather than capturing CO<sub>2</sub> to form organic or inorganic carbonates, particularly when exposed to ambient air.

Strategies including molecular engineering,<sup>[8, 21]</sup> electrolyte engineering,<sup>[3, 18-20, 23]</sup> and electrochemical engineering<sup>[11]</sup> have been employed to address the O<sub>2</sub> sensitivity issue of the redox-active sorbents in their reduced state, leading to significant advancements in point source capture. However, the inherent O<sub>2</sub> sensitivity issue of the redox-active sorbents at the molecular level persists. As a result, the viability of using redox-active sorbents for electrochemically induced DAC remains an open question.

Ribulose-1,5-bisphosphate (RuBP) in plant leaves preferentially reacts with CO<sub>2</sub> over O<sub>2</sub> in the sunlight, despite the orders of magnitude difference in partial pressures—0.4 mbar CO<sub>2</sub> vs. 0.21 bar O<sub>2</sub> in air.<sup>[26]</sup> Motivated by the capability of RuBP in carbon fixation through photosynthesis, we envision the possibility of developing a redox-active sorbent capable of electrochemically induced DAC while tolerating ambient oxygen.

Fluoroflavine, an azaacene dye known for its intense fluorescence,<sup>[27, 28]</sup> has been used to facilitate charge transfer in LiFePO<sub>4</sub> and used as an electro-active material for energy storage.<sup>[29, 30]</sup> Our interest in fluoroflavine stems from its unique properties, including its air stability,<sup>[30]</sup> high pKa values,<sup>[31]</sup> and excellent redox activity.<sup>[27]</sup> Through introducing water-solubilizing sulfonate groups to fluoroflavine, we developed an oxygen-tolerant aqueous-soluble fluoroflavine disulfonate sorbent that can be electrochemically induced to capture CO<sub>2</sub> from simulated flue gas as well as indoor and outdoor ambient air, with low energy cost, excellent reversibility, and high stability. The electrochemically induced CO<sub>2</sub> capture system with aqueous redox-active sorbents inherits the merits of aqueous flow batteries, including non-flammability, continuous-flow engineering, modularity, and the ability to operate at high current densities. We demonstrated that increasing the applied current densities accelerates the CO<sub>2</sub> capture-release rate, which is crucial in addressing the urgent challenge of climate change.

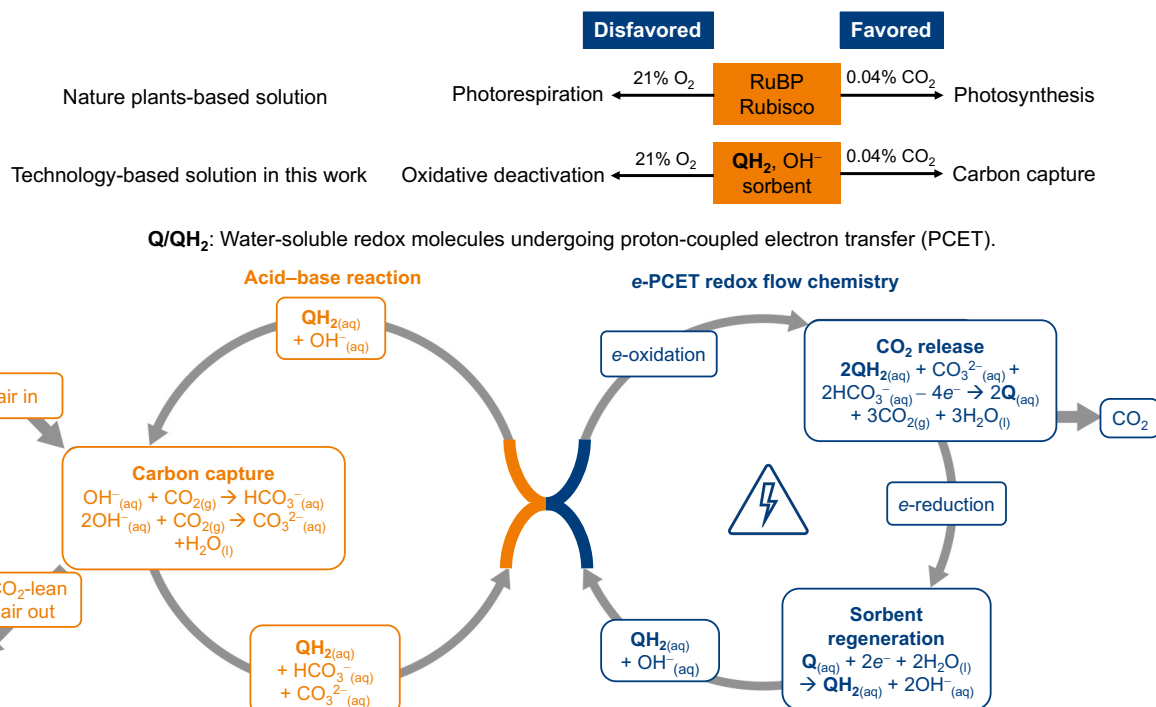


**Figure 1 |** Schematics of nature-based DAC solution and technology-based DAC solution in this work. Both DAC solutions face a vast difference in partial pressures between O<sub>2</sub> and CO<sub>2</sub>, 0.21 bar vs. 0.4 mbar. In the presence of light, RuBP and Rubisco preferentially react with CO<sub>2</sub> over O<sub>2</sub>, promoting photosynthesis over photorespiration. The redox-active sorbents used in the emerging electrochemically induced DAC technology usually encounter an oxygen sensitivity issue and show poor selectivity for CO<sub>2</sub> over O<sub>2</sub>. Ideally, a redox-active sorbent Q (QH<sub>2</sub>), with inherent oxygen tolerance at molecular level, would enable electrochemically induced carbon capture from the air, while greatly suppressing the sorbent oxidative deactivation. Three steps are involved in Q/QH<sub>2</sub> sorbent-based CO<sub>2</sub> capture and

release: 1. acid–base reaction induced CO<sub>2</sub> capture; 2. electrochemically induced CO<sub>2</sub> release; 3. electrochemical reduction for sorbent regeneration.

## Results and discussion

Fluoflavine (**FF**) was synthesized through a condensation reaction.<sup>[30]</sup> After the one-step sulfonation of **FF**, we obtained fluoflavine disulfonic acid (**FFDS**) with an outstanding yield of 94%. The disulfonation of **FF** was confirmed by the mass-to-charge ratio obtained from high-resolution mass spectrometry. The oxidized **FFDS** (**ox. FFDS**) was quantitatively obtained through a one-step electrochemical oxidation. By analysing the splitting pattern and the ratio of peak integrals in the aromatic regions of their <sup>1</sup>H NMR spectra, we were able to determine the structure of **FFDS** and **ox. FFDS** as drawn in **Figure 2a**, where the two sulfonate groups are attached to the separated phenyl rings at the meta- or para-positions. The number of peaks in the <sup>13</sup>C NMR spectra further validates the proposed structures.

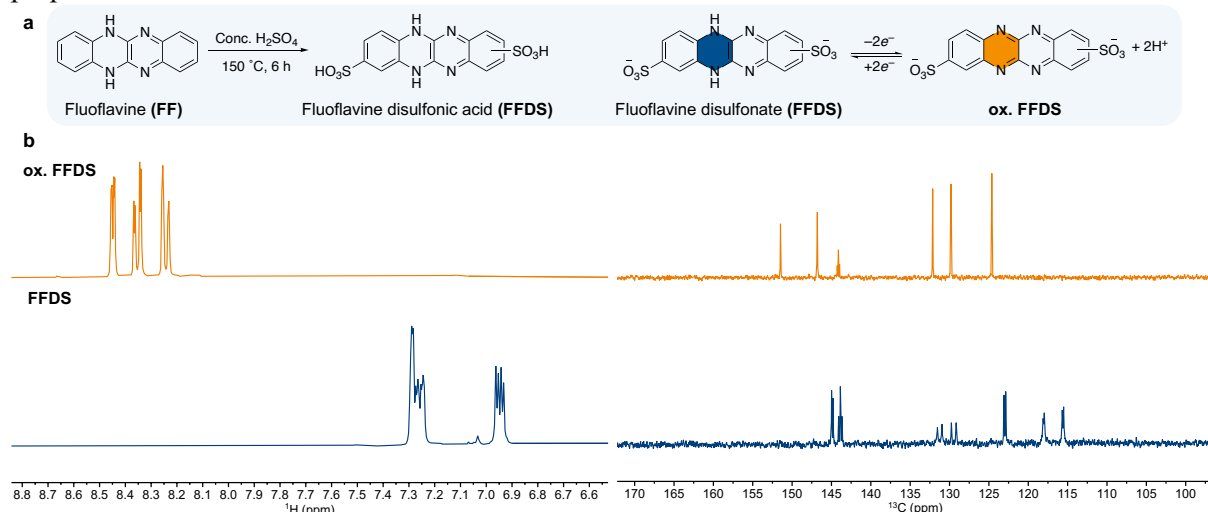


**Figure 2 |** Synthesis and NMR spectra of fluoflavine disulfonate (**FFDS**) and its oxidized form (**ox. FFDS**). **a**, Fluoflavine sulfonation reaction condition and the electrochemical proton-coupled electron transfer (PCET). **b**, <sup>1</sup>H and <sup>13</sup>C NMR spectra of the **ox. FFDS** and **FFDS** in DMSO-*d*<sub>6</sub>. See **Figure S1–S2** for more details.

The cyclic voltammograms of **FFDS** in buffered aqueous media exhibit reversible redox behaviour over a pH range of 5.7 to 13.9 (**Figure 3a**). The Pourbaix diagram in **Figure 3b** indicates that the redox potential of **FFDS** is negatively proportional to pH with a fitted slope of 59 mV/pH throughout the pH range from 0 to 14. The overlap between the experimental reduction potentials of **FFDS** and the theoretical values (**Figure S10**) further corroborates that **FFDS** undergoes two-proton, two-electron transfer, *i.e.*, proton-coupled electron transfer (PCET), over the pH range of 0 to 14. It is worth noting that the oxidation potentials of **FFDS** fall between the potentials of two-electron transfer oxygen reduction reaction (ORR) and four-electron transfer ORR (**Figure 3b**). Given that the four-electron transfer ORR pathway is highly disfavoured in the absence of a catalyst, **FFDS** could potentially tolerate ambient O<sub>2</sub>, thus enabling **FFDS** sorbent-based electrochemically induced DAC.

The electrochemically induced CO<sub>2</sub> capture using **FFDS** was first examined in the absence of O<sub>2</sub>. **FFDS** shows a reversible swing in both pH and potential while operating in N<sub>2</sub> (**Figure 3c**). The introduction of CO<sub>2</sub> to the reduced electrolyte leads to a steep decline in pH and a sharp rise in potential, which are attributed to the CO<sub>2</sub> buffering effect (**Figure 3d**). A slight pH increase and potential drop are observed after the CO<sub>2</sub> feed gas is replaced by pure N<sub>2</sub>. Such a phenomenon can be explained by the CO<sub>2</sub> partial pressure drop in feed gas lowering the solubility of CO<sub>2</sub> in liquid phase. Subsequent oxidation of **FFDS** lowers the electrolyte pH from 9.5 to 4, accompanied by the CO<sub>2</sub> release. The replotted voltage profiles in **Figure 3e** clearly show that the oxidation potential of **FFDS** shifts to a more positive value after CO<sub>2</sub> capture. The integrated loop area in **Figure 3f** represents the energy required for CO<sub>2</sub> release and **FFDS** sorbent regeneration. With a one-hour exposure of pure CO<sub>2</sub> at one

bar, the **FFDS** sorbent could release 43.10 mL CO<sub>2</sub> after the electrochemical oxidation (**Figure S5**), which corresponds to a CO<sub>2</sub>/e molar ratio of 0.97 and an energy cost of 32.97 kJ mol<sup>-1</sup> CO<sub>2</sub>.

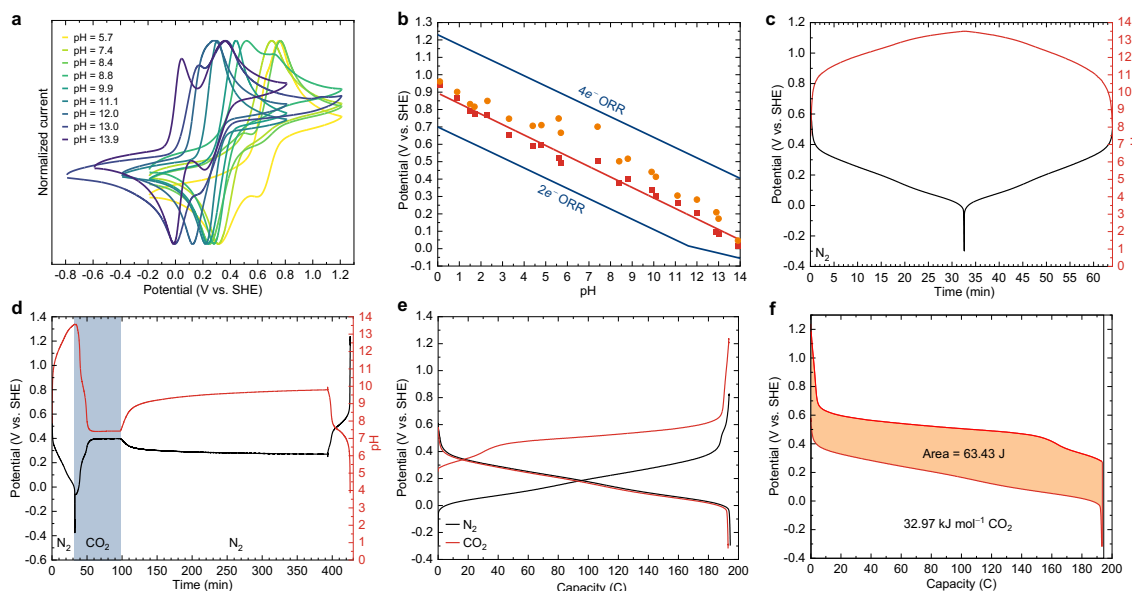


**Figure 3 |** Electrochemical characterizations of **FFDS** in the absence and presence of CO<sub>2</sub>. **a**, Cyclic voltammograms of **FFDS** in buffered electrolytes. **b**, Pourbaix diagram of **FFDS**. **c**, Potential and pH profiles of **FFDS** electrolyte over time in N<sub>2</sub>. **d**, Potential and pH profiles of **FFDS** electrolyte over time when CO<sub>2</sub> is introduced. **e**, Potential vs. capacity profiles with and without captured CO<sub>2</sub>. **f**, Energy cost for CO<sub>2</sub> release and sorbent regeneration when CO<sub>2</sub> is captured from one-bar 100% CO<sub>2</sub>.

In light of the distinctive colours of the azaacene family<sup>[27, 28]</sup>, we carried out spectroscopic studies on **FFDS** at varied state of charge (SOC). **Figure 4a** shows that the UV–Vis absorbance spectrum of **FFDS** evolves reversibly between 0% and 100% SOC, confirming the reversible redox behaviour. Although the structural conjugation is extended from **FFDS** to **ox. FFDS**, the corresponding UV–Vis spectral shift is insignificant, which has also been corroborated by the simulated results (**Figure S7**). The lack of red shift can be attributed to the fact that the S<sub>0</sub>–S<sub>1</sub> transition is forbidden due to the substantial alternation in molecular symmetry caused by oxidation (**Figure S8**).

As implied by the name, fluorescence is an inherent feature of fluoflavine derivatives. The fluorescence of **FFDS** linearly diminishes with the decrease of SOC (**Figure 4b**). The same linear correlation has also been observed in the mixture of **FFDS** and **ox. FFDS** in varying ratios (**Figure S12**). It is important to note that the quantitative relationship between fluorescence intensity and SOC could be established via *in-situ* non-invasive fluorescence technique.<sup>[32]</sup> The almost non-fluorescent feature shown by the **ox. FFDS** can also be attributed to the S<sub>0</sub>–S<sub>1</sub> transition being forbidden. The fluorescence of the **ox. FFDS** is effectively quenched by rapid internal conversion to the dark state (S<sub>1</sub>) upon photoexcitation, as confirmed by the transient absorption measurements (**Figure S13**). The **FFDS** solutions with and without captured CO<sub>2</sub> show the same spectra of both UV–Vis absorbance and fluorescence (**Figure S11–S12**), indicating that CO<sub>2</sub> is captured as dissolved inorganic carbon (DIC) species that does not affect the structure of **FFDS**, validating that **FFDS** captures and releases CO<sub>2</sub> via pH-swing rather than nucleophilicity-swing.<sup>[5, 15]</sup>

The *in-situ* ATR-FTIR spectra of **FFDS** over the electrochemical reduction process in **Figure 4c** show gradual transmittance variations at 1150–1200, 1600, 2900, and 3200–3300 cm<sup>-1</sup>, which correspond to the stretching vibrations of C–N, C=N, N–H, and O–H bonds, respectively.<sup>[21, 33, 34]</sup> During the reduction, the C=N bonds in one of the two pyrazine rings are converted to C–N and N–H bonds, intensifying the absorption bands at 1150, 1200, and 2900 cm<sup>-1</sup>, weakening the C=N absorption band at 1600 cm<sup>-1</sup>. The O–H vibration absorption in the range of 3200–3300 cm<sup>-1</sup> diminishes, as water molecules are consumed over reduction.

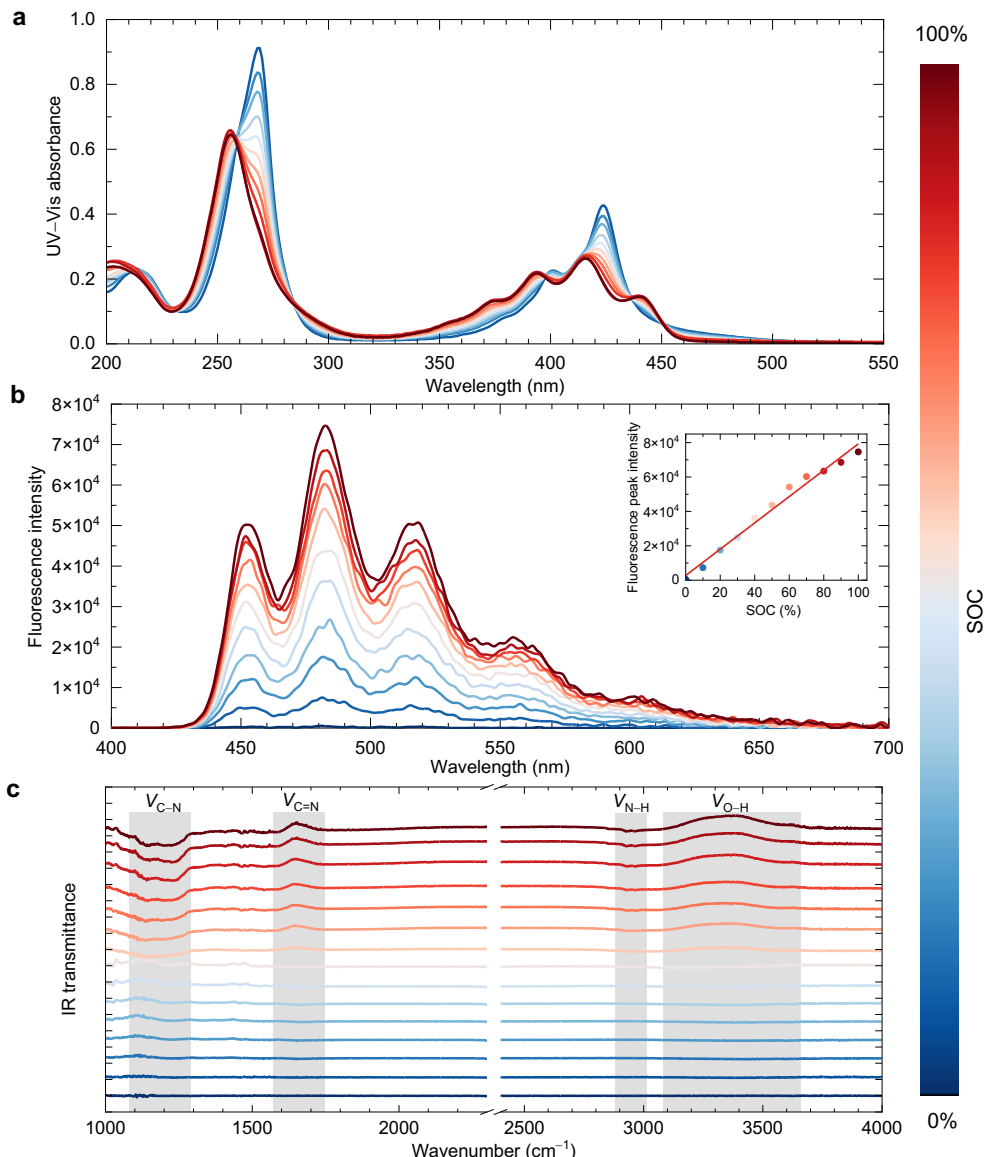


**Figure 4** | Spectroscopic studies of  $10\text{ }\mu\text{M}$  **FFDS**. **a**, UV–Vis absorbance spectra at varied SOC between 0% and 100%. **b**, Fluorescence emission spectra of **FFDS** at varied SOC, and the fluorescence peak intensity vs. SOC (insert). **c**, Stacked *in-situ* IR transmittance spectra of **FFDS** over electrochemical reduction process (bottom to top: 0% to 100% SOC).

To assess the oxygen tolerance of **FFDS**, we measured the  $\text{CO}_2$  capture performance of **FFDS** sorbent in a simulated flue gas consisting of 10%  $\text{CO}_2$ , 10%  $\text{O}_2$ , and 80%  $\text{N}_2$  at one bar. The simulated flue gas is introduced to the **FFDS** electrolyte as the feed gas at a flow rate of  $30\text{ mL min}^{-1}$ . The flow cell is charged to electrochemically reduce **ox. FFDS**, thereby regenerating the sorbent. The pH of the sorbent first increases from 7.25 to 9.5, then decreases and stabilizes at 7.7 which is a result of the acid–base reaction between the  $\text{CO}_2$  in the feed gas and the  $\text{OH}^-$  generated via the PCET process. Correspondingly, the  $\text{CO}_2$  flow rate becomes lower than  $3\text{ mL min}^{-1}$ ; while the oxygen level becomes higher than 10%. The acid–base reaction-induced  $\text{CO}_2$  capture continues after the charging process and completes during the rest period. During the electrochemical oxidation of **FFDS**, the pH of the sorbent first decreases from 7.7 to 6.6, then increases and stabilizes at 7.25. The corresponding  $\text{CO}_2$  release leads to the increase of  $\text{CO}_2$  flow rate and the decrease of  $\text{O}_2$  level. The reversible alterations in voltage, pH,  $\text{O}_2$  level, and  $\text{CO}_2$  capture flow rate over 11 cycles indicate the excellent oxygen tolerance of **FFDS** in 0.1 bar  $\text{O}_2$  (**Figure 5a**). Being exposed to 0.1 bar  $\text{O}_2$  for 200-hour, 38-cycle  $\text{CO}_2$  capture and release, the **FFDS** sorbent steadily releases  $\text{CO}_2$  at an average volume of  $36.7\text{ mL}$  per cycle with an average

Coulombic efficiency of 99.02% (**Figure 5b**, **Figure S20**), indicating that FFDS possesses exclusive selectivity of CO<sub>2</sub> over O<sub>2</sub>, superior oxygen-tolerance, and excellent reversibility. The molar ratio of CO<sub>2</sub>/e approaching 0.88 suggests that CO<sub>2</sub> was primarily absorbed via the reaction of CO<sub>2</sub> + OH<sup>-</sup> → HCO<sub>3</sub><sup>-</sup> during the capture process, which is also reflected by the stabilized pH at 7.7 after the completion of CO<sub>2</sub> capture. As shown in **Figure S16**, the DIC in water at pH 7.7 is primarily in the form of bicarbonate.

It is worth noting that the aqueous electrochemical flow system is capable of operating at high current densities, thus accelerating the CO<sub>2</sub> release and sorbent regeneration, ultimately expediting the DAC rate. **Figure 5c** shows the averaged volumes of CO<sub>2</sub> capture–release over five cycles at varied current densities. Increasing the applied current densities does not adversely lower the volumes of CO<sub>2</sub> captured and released by the FFDS sorbent. Instead, it reduces the time required to complete the CO<sub>2</sub> capture from 132 to 92 minutes when the applied current density increases from 20 to 40 mA cm<sup>-2</sup> (**Figure S21b**). Further increasing the current density does not shorten the CO<sub>2</sub> capture time, as the rate-limiting step becomes the acid–base chemical reaction between CO<sub>2</sub> and OH<sup>-</sup>. **Figure 5d** shows that the CO<sub>2</sub> release peak intensifies with the increase of current densities, shortening the duration of CO<sub>2</sub> capture–release cycle. Because CO<sub>2</sub> release is coupled with electrochemical oxidation of FFDS, increasing the applied current densities from 20 to 100 mA cm<sup>-2</sup> reduces the time required to complete CO<sub>2</sub> release from 50 to 20 mins (**Figure 5e**). **Figure 5f** shows the comparable Coulombic efficiencies of close to 100% and the increased energy cost for CO<sub>2</sub> release and sorbent regeneration from 58 to 190 kJ mol<sup>-1</sup> CO<sub>2</sub> when the applied current density is increased from 20 to 100 mA cm<sup>-2</sup>.

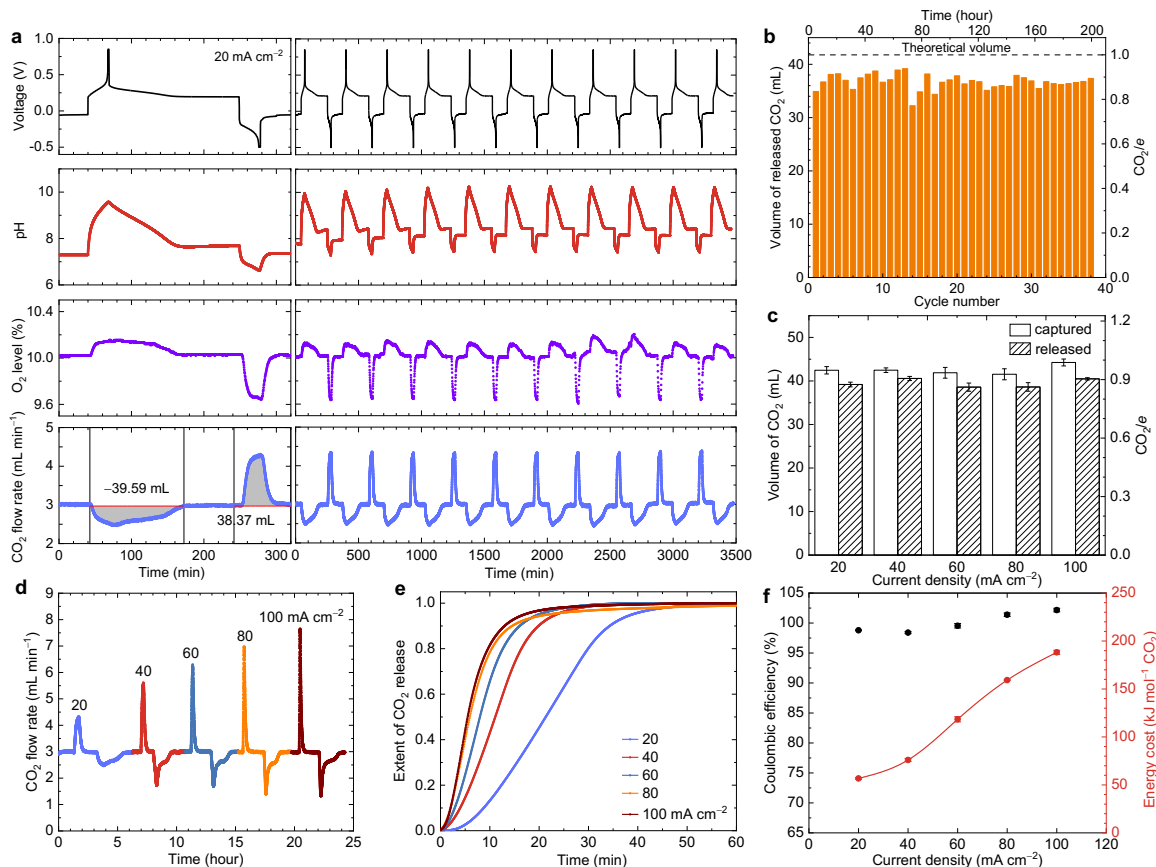


**Figure 5 |** FFDS sorbent-based electrochemically induced CO<sub>2</sub> capture and release at one bar in a simulated flue gas composed of 10% CO<sub>2</sub>, 10% O<sub>2</sub> and 80% N<sub>2</sub> at a total flow rate of 30 mL min<sup>-1</sup>. The negolyte is composed of 10 mL of 0.1 M FFDS, 0.4 M KOH. The posolyte is composed of 100 mL of 0.03 M K<sub>4</sub>Fe(CN)<sub>6</sub> and 0.07 M K<sub>3</sub>Fe(CN)<sub>6</sub>. The flow cell is charged–discharged at constant current densities with potential holds until the current density decreases to 2 mA cm<sup>-2</sup>. A 180-min rest after charge, and a 90-min rest after discharge are implemented to complete CO<sub>2</sub> capture and release, respectively. **a**, One-cycle and 10-cycle CO<sub>2</sub> capture and release at 20 mA cm<sup>-2</sup>. Top to bottom: voltage profile, variation of pH, O<sub>2</sub> level, and CO<sub>2</sub> flow rate. **b**, Volume of released CO<sub>2</sub>, molar ratio of CO<sub>2</sub>/e

at 20 mA cm<sup>-2</sup> over 38 cycles and 200 hours. **c**, Volume of released CO<sub>2</sub>, molar ratio of CO<sub>2</sub>/e at 20, 40, 60, 80, and 100 mA cm<sup>-2</sup> over five cycles. **d**, CO<sub>2</sub> capture and release at varied current densities of 20, 40, 60, 80, and 100 mA cm<sup>-2</sup>. **e**, Cumulative CO<sub>2</sub> released over time at 20, 40, 60, 80, and 100 mA cm<sup>-2</sup>. **f**, Averaged Coulombic efficiency and energy cost over five cycles at 20, 40, 60, 80, and 100 mA cm<sup>-2</sup>.

Encouraged by the stable cycling of carbon capture and release in the simulated flue gas, we put 10 mL, 0.1 M **FFDS** sorbent in the indoor air and stirred it for three days. As such, we were able to evaluate the outcome of the two competing reactions—carbon capture vs. oxidative deactivation of **FFDS** (**Figure 1**) over an extended air exposure. Instead of releasing CO<sub>2</sub> to a mixed gas containing 10% CO<sub>2</sub> at ambient pressure (**Figure 5**), we employed pure N<sub>2</sub> (99.9995%) as the carrier gas to avoid any further unintended CO<sub>2</sub> capture, as the sorbent after DAC would immediately continue to capture CO<sub>2</sub> upon being exposed to a feed gas containing 0.1 bar CO<sub>2</sub>, which ultimately leads to an overestimation in DAC capacity and the CO<sub>2</sub>/e molar ratio. **Figure 6b** shows the charge–discharge voltage profile of **FFDS** after the three-day DAC. A Coulombic efficiency of 87% suggests that most of **FFDS** remains intact after the three-day indoor air exposure. 20.16 mL CO<sub>2</sub> is released (**Figure 6d**), corresponding to a CO<sub>2</sub>/e molar ratio of 0.51.

To assess the cycling stability of **FFDS** sorbent-based DAC and release, we conducted 10 cycles of continuous three-day indoor DAC plus one-day CO<sub>2</sub> release, as shown in **Figure 6h**. During the 40 days of operation, the **FFDS** sorbent releases 16.5–20.0 mL CO<sub>2</sub> per cycle with a Coulombic efficiency of 85–95% and an energy cost of 80–110 kJ mol<sup>-1</sup> for CO<sub>2</sub> release and sorbent regeneration. The variation in the released CO<sub>2</sub> volume is mainly attributed to sorbent loss or residual sorbent left behind during transfer.

Although the significantly improved oxygen tolerance of **FFDS** enables us to capture CO<sub>2</sub> from the air, there is still 5–15% of **FFDS** being oxidized by molecular oxygen during the three-day air exposure, as reflected by the Coulombic efficiency. As a result, part of the captured CO<sub>2</sub> remains in the sorbent solution. The remaining DIC creates a buffer solution that stabilizes its pH at 9.3 after CO<sub>2</sub> release and at 12.6 after the sorbent regeneration (**Figure 6c**). To confirm whether the DICs accumulate over cycling, 1 M HCl was intentionally added to the cycled **FFDS** sorbent (**Figure S24**), and a total of 36 mL CO<sub>2</sub> was released, validating our reasoning. However, the addition of hydrochloric acid adversely introduces extra ions to the sorbent, which would compromise the aqueous solubility of **FFDS**. Furthermore, the unbalanced charges over cycling will eventually outbalance the whole system.

To eliminate the influence of extra ions and rebalance the charges in the system,<sup>[11, 35]</sup> we further lowered the discharge voltage to initiate the oxygen evolution reaction (OER), which was noted as deep discharge. By controlling the deep discharge capacity, we improved the Coulombic efficiency close to 100% and increased the initial CO<sub>2</sub> release volume up to 23.31 mL. With the controlled OER, we lowered the pH to 4.0 after CO<sub>2</sub> release to ensure that no HCO<sub>3</sub><sup>-</sup> and CO<sub>3</sub><sup>2-</sup> were left in the sorbent (**Figure S16**). The subsequent charge process elevates the sorbent pH up to 13.3. To accelerate the DAC–release cycle, we kept bubbling the sorbent solution with the indoor air overnight at a flow rate of 375 mL min<sup>-1</sup> and stopped bubbling when the sorbent pH decreased to ~10. The whole DAC–release cycle completes within one day. **Figure 6i** shows the cycling over 16 days with an average CO<sub>2</sub> release volume of 21.6 mL. The fluctuation in the volume of released CO<sub>2</sub> was mainly due to the unavoidable liquid splashes caused by air bubbling. Compared to the normal discharge, the deep discharge method improves the Coulombic efficiency close to 100%, releases 3.2 mL more CO<sub>2</sub>, and rebalances the system with 51% higher energy cost (**Figure 6i** vs. **Figure 6h**).

With the 0.2 M **FFDS** sorbent, we conducted both indoor and outdoor DAC in Singapore, a city country near the equator with a tropical climate of high humidity and relatively consistent temperatures year-round. **Figure 6a** presents the continuous 20-day indoor and outdoor temperatures, relative humidity, oxygen, and CO<sub>2</sub> levels of Singapore in Feb. 2025. The outdoor open air shows recurring oscillations for all of the monitored parameters. Because of air conditioning, the indoor air is maintained at relatively stable temperature, humidity, and O<sub>2</sub> levels. The indoor CO<sub>2</sub> fluctuation is due to the activities of group members. **Figure 6j** presents the continuous cycling of **FFDS** sorbent for two cycles of the three-day indoor DAC, and another two cycles of the three-day outdoor DAC. The **FFDS** sorbent releases more than 46 mL CO<sub>2</sub> after the three-day indoor and outdoor DAC, doubling the DAC capacity

as compared to the 0.1 M **FFDS** sorbent. The similar released CO<sub>2</sub> volumes, Coulombic efficiency, and energy cost indicate that the fluctuations in temperature and humidity levels of the outdoor air have insignificant influence on the **FFDS** sorbent. It is noticed that the water loss from the **FFDS** sorbent during the three-day outdoor DAC is 30%–50% less than that during the three-day indoor DAC. The 10% higher relative humidity in the outdoor air slows down the water evaporation of **FFDS** sorbent during the three-day outdoor DAC (**Figure 6a**).

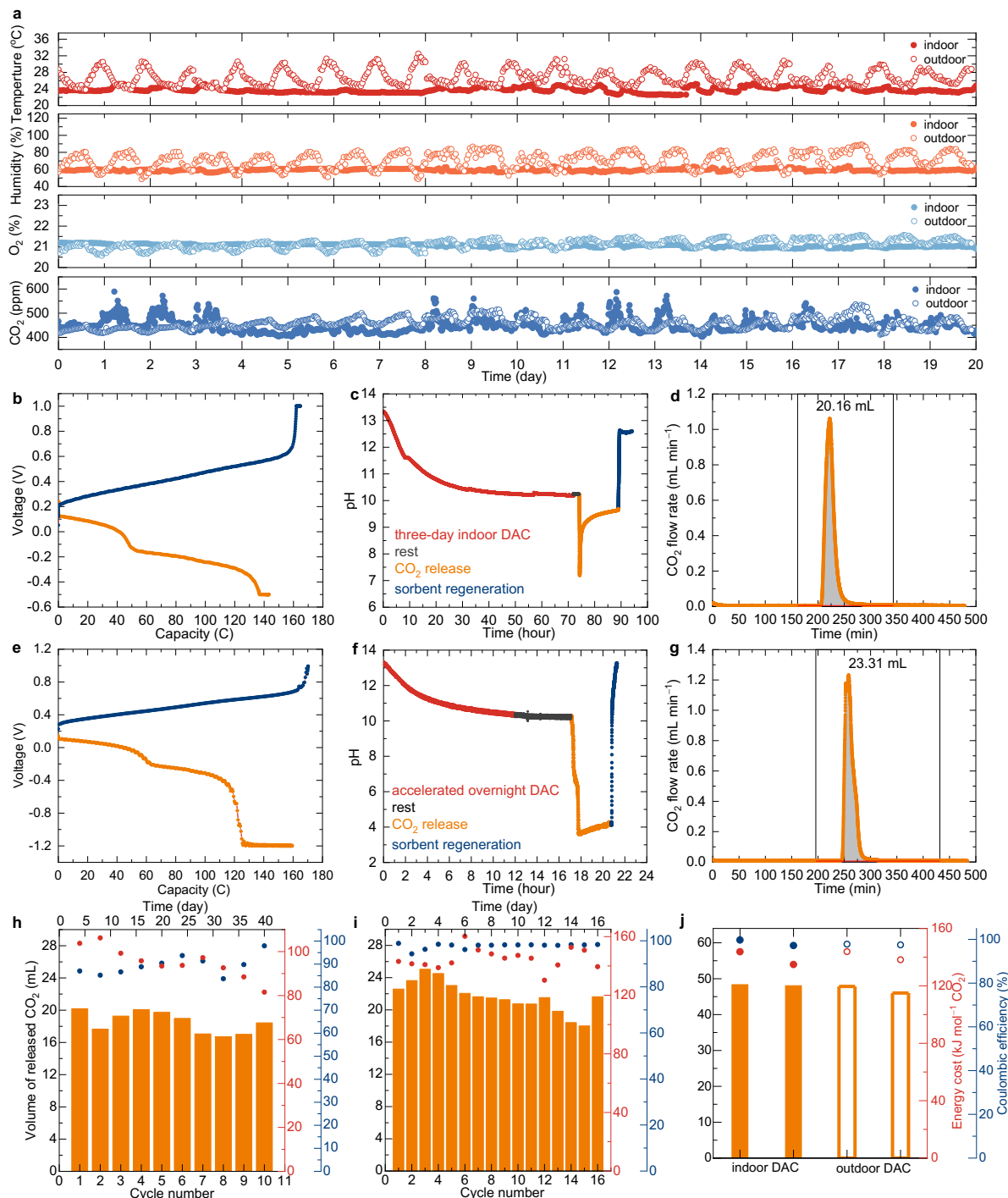


**Figure 6 | FFDS** sorbent-based electrochemically induced DAC and CO<sub>2</sub> release from both indoor and outdoor ambient air in Singapore. 10 mL, 0.1 M **FFDS** and 0.4 M KOH was used as the sorbent for the experiments in **a–i**. The posolyte is composed of 100 mL of 0.03 M K<sub>4</sub>Fe(CN)<sub>6</sub> and 0.07 M K<sub>3</sub>Fe(CN)<sub>6</sub>. The flow cell is charged-discharged at 20 mA cm<sup>-2</sup> with potential holds until the current density decreases to 2 mA cm<sup>-2</sup>. **a**, Indoor and outdoor air monitoring including temperature, relative humidity, O<sub>2</sub> and CO<sub>2</sub> levels for 20 days. **b**, Normal discharge–charge voltage profile. **c**, pH monitoring during

the three-day indoor DAC, rest, CO<sub>2</sub> release, and the sorbent regeneration. **d**, Variation in CO<sub>2</sub> flow rate over CO<sub>2</sub> release with normal discharge. **e**, Deep discharge–charge voltage profile. **f**, pH monitoring during the three-day indoor DAC, rest, CO<sub>2</sub> release, and the sorbent regeneration. **g**, Variation in CO<sub>2</sub> flow rate over CO<sub>2</sub> release with deep discharge. **h**, 10 cycles of normal discharge induced CO<sub>2</sub> release after the three-day indoor DAC over 40 days. **i**, 16 cycles of deep discharge induced CO<sub>2</sub> release after the accelerated overnight indoor DAC. **j**, Comparison of the three-day indoor and outdoor DAC with the 10 mL, 0.2 M **FFDS** sorbent. The posolyte is composed of 200 mL of 0.03 M K<sub>4</sub>Fe(CN)<sub>6</sub> and 0.07 M K<sub>3</sub>Fe(CN)<sub>6</sub>.

Depending on the discharge voltage cutoffs, **FFDS**-sorbent used for electrochemically induced DAC exhibits an estimated energy cost range of 3.15–6.14 GJ tonne<sup>-1</sup> CO<sub>2</sub> when air contact, CO<sub>2</sub> release, sorbent regeneration, and pressurization are taken into consideration (**Table S5**), which is significantly lower than the hydroxide solution-based thermochemical approach.<sup>[2]</sup> Furthermore, among the reported technology-based DAC solutions operating at ambient pressure, the **FFDS** sorbent bears the lowest energy cost for CO<sub>2</sub> release and sorbent regeneration (**Table S6**).

## Outlook

We developed an aqueous-soluble, oxygen-tolerant fluoflavine sorbent that can be electrochemically induced to capture CO<sub>2</sub> from simulated flue gas, as well as indoor and outdoor ambient air. Specifically, we synthesized an aqueous soluble fluoflavine disulfonate **FFDS** in a one-step sulfonation with an outstanding yield. Electrochemical characterizations, theoretical calculations, and spectroscopic studies reveal that **FFDS** not only undergoes reversible two-proton, two-electron transfer, but also exhibits an oxidation potential exceedingly higher than that of the two-electron transfer oxygen reduction reaction across the entire pH range of 0 to 14, indicating that **FFDS** can potentially capture and release CO<sub>2</sub> via pH-swing in the presence of O<sub>2</sub>. In a one-bar simulated flue gas containing 10% CO<sub>2</sub>, 10% O<sub>2</sub>, and 80% N<sub>2</sub>, the **FFDS** sorbent shows a reversible CO<sub>2</sub> capture and release with an average CO<sub>2</sub>/e molar ratio of 0.88 and a Coulombic efficiency of >99% throughout 38 cycles and 200 hours. Besides, as the applied current density increases, the discharge-induced CO<sub>2</sub> release rate is substantially accelerated. Throughout the 10-cycle three-day indoor DAC over the course of 40 days, **FFDS** shows an average Coulombic efficiency of 90% via a normal discharge–charge process and releases 16.5–20.0 mL of CO<sub>2</sub>. Instead of stirring the sorbent in the air for three days, we continuously passed ambient air through the sorbent solution overnight to expedite the DAC process and implemented a deep discharge step to fully release the captured CO<sub>2</sub>, achieving a steady DAC–CO<sub>2</sub> release with an improved Coulombic efficiency of ~99% over 16 cycles. The **FFDS** sorbent shows an inappreciable difference in its CO<sub>2</sub> capture and release capacity between the indoor and outdoor DAC, in spite of the elevated and fluctuating temperature and humidity levels outdoors in Singapore. The CO<sub>2</sub> capture capacity increases twofold when the concentration of **FFDS** is doubled, regardless of whether the DAC is conducted indoors or outdoors. Molecular engineering could be employed to further improve the aqueous solubility, structural stability, and oxygen tolerance of the fluoflavine derivatives. Electrochemical and electrolyte optimizations would maximize the CO<sub>2</sub> capture capacity, lower the energy cost, and expedite the DAC rate at high current densities.

## References

- [<sup>1</sup>]G.T. Rochelle, "Amine Scrubbing for CO<sub>2</sub> Capture", *Science* **325**, 1652 (2009). <https://doi.org/10.1126/science.1176731>
- [<sup>2</sup>]D.W. Keith, G. Holmes, D. St. Angelo, and K. Heidel, "A Process for Capturing CO<sub>2</sub> from the Atmosphere", *Joule* **2**, 1573 (2018). <https://doi.org/10.1016/j.joule.2018.05.006>
- [<sup>3</sup>]B. Gurkan, F. Simeon, and T.A. Hatton, "Quinone Reduction in Ionic Liquids for Electrochemical CO<sub>2</sub> Separation", *ACS Sustainable Chemistry & Engineering* **3**, 1394 (2015). <https://doi.org/10.1021/acssuschemeng.5b00116>
- [<sup>4</sup>]M. Rahimi, G. Catalini, S. Hariharan, M. Wang, M. Puccini, and T.A. Hatton, "Carbon Dioxide Capture Using an Electrochemically Driven Proton Concentration Process", *Cell Reports Physical Science* **1**, (2020). <https://doi.org/10.1016/j.xrpp.2020.100033>

- [<sup>5</sup>] S. Jin, M. Wu, R.G. Gordon, M.J. Aziz, and D.G. Kwabi, "Ph Swing Cycle for CO<sub>2</sub> capture Electrochemically Driven through Proton-Coupled Electron Transfer", *Energy & Environmental Science* **13**, 3706 (2020). <https://doi.org/10.1039/d0ee01834a>
- [<sup>6</sup>] H. Xie, W. Jiang, T. Liu, Y. Wu, Y. Wang, B. Chen, D. Niu, and B. Liang, "Low-Energy Electrochemical Carbon Dioxide Capture Based on a Biological Redox Proton Carrier", *Cell Reports Physical Science* **1**, (2020). <https://doi.org/10.1016/j.xrpp.2020.100046>
- [<sup>7</sup>] R. Sharifian, R.M. Wagterveld, I.A. Digdaya, C. Xiang, and D.A. Vermaas, "Electrochemical Carbon Dioxide Capture to Close the Carbon Cycle", *Energy & Environmental Science* **14**, 781 (2021). <https://doi.org/10.1039/d0ee03382k>
- [<sup>8</sup>] J.M. Barlow, L.E. Clarke, Z. Zhang, D. Bim, K.M. Ripley, A. Zito, F.R. Brushett, A.N. Alexandrova, and J.Y. Yang, "Molecular Design of Redox Carriers for Electrochemical CO<sub>2</sub> Capture and Concentration", *Chem. Soc. Rev.* **51**, 8415 (2022). <https://doi.org/10.1039/d2cs00367h>
- [<sup>9</sup>] K.M. Diederichsen, R. Sharifian, J.S. Kang, Y. Liu, S. Kim, B.M. Gallant, D. Vermaas, and T.A. Hatton, "Electrochemical Methods for Carbon Dioxide Separations", *Nature Reviews Methods Primers* **2**, (2022). <https://doi.org/10.1038/s43586-022-00148-0>
- [<sup>10</sup>] C. Huang, C. Liu, K. Wu, H. Yue, S. Tang, H. Lu, and B. Liang, "CO<sub>2</sub> Capture from Flue Gas Using an Electrochemically Reversible Hydroquinone/Quinone Solution", *Energy & Fuels* **33**, 3380 (2019). <https://doi.org/10.1021/acs.energyfuels.8b04419>
- [<sup>11</sup>] S. Jin, M. Wu, Y. Jing, R.G. Gordon, and M.J. Aziz, "Low Energy Carbon Capture Via Electrochemically Induced pH Swing with Electrochemical Rebalancing", *Nature Communications* **13**, (2022). <https://doi.org/10.1038/s41467-022-29791-7>
- [<sup>12</sup>] H. Seo, M. Rahimi, and T.A. Hatton, "Electrochemical Carbon Dioxide Capture and Release with a Redox-Active Amine", *J. Am. Chem. Soc.* **144**, 2164 (2022). <https://doi.org/10.1021/jacs.1c10656>
- [<sup>13</sup>] S. Pang, S. Jin, F. Yang, M. Alberts, L. Li, D. Xi, R.G. Gordon, P. Wang, M.J. Aziz, and Y. Ji, "A Phenazine-Based High-Capacity and High-Stability Electrochemical CO<sub>2</sub> Capture Cell with Coupled Electricity Storage", *Nature Energy* **8**, 1126 (2023). <https://doi.org/10.1038/s41560-023-01347-z>
- [<sup>14</sup>] H. Seo and T.A. Hatton, "Electrochemical Direct Air Capture of CO<sub>2</sub> Using Neutral Red as Reversible Redox-Active Material", *Nature Communications* **14**, (2023). <https://doi.org/10.1038/s41467-023-35866-w>
- [<sup>15</sup>] Y. Jing, K. Amini, D. Xi, S. Jin, A.M. Alfaraidi, E.F. Kerr, R.G. Gordon, and M.J. Aziz, "Electrochemically Induced CO<sub>2</sub> Capture Enabled by Aqueous Quinone Flow Chemistry", *ACS Energy Letters* **9**, 3526 (2024). <https://doi.org/10.1021/acsenergylett.4c01235>
- [<sup>16</sup>] S. Liu, J. Zhang, F. Li, J.P. Edwards, Y.C. Xiao, D. Kim, P. Papangelakis, J. Kim, D. Elder, P. De Luna, M. Fan, G. Lee, R.K. Miao, T. Ghosh, Y. Yan, Y. Chen, Y. Zhao, Z. Guo, C. Tian, P. Li, Y. Xu, E.H. Sargent, and D. Sinton, "Direct Air Capture of CO<sub>2</sub> via Cyclic Viologen Electrocatalysis", *Energy & Environmental Science* **17**, 1266 (2024). <https://doi.org/10.1039/d3ee03024e>
- [<sup>17</sup>] S. Voskian and T.A. Hatton, "Faradaic Electro-Swing Reactive Adsorption for CO<sub>2</sub> Capture", *Energy & Environmental Science* **12**, 3530 (2019). <https://doi.org/10.1039/c9ee02412c>
- [<sup>18</sup>] Y. Liu, H.Z. Ye, K.M. Diederichsen, T. Van Voorhis, and T.A. Hatton, "Electrochemically Mediated Carbon Dioxide Separation with Quinone Chemistry in Salt-Concentrated Aqueous Media", *Nat. Commun.* **11**, 2278 (2020). <https://doi.org/10.1038/s41467-020-16150-7>
- [<sup>19</sup>] J.M. Barlow and J.Y. Yang, "Oxygen-Stable Electrochemical CO<sub>2</sub> Capture and Concentration with Quinones Using Alcohol Additives", *J. Am. Chem. Soc.* **144**, 14161 (2022). <https://doi.org/10.1021/jacs.2c04044>
- [<sup>20</sup>] K.M. Diederichsen, Y. Liu, N. Ozbek, H. Seo, and T.A. Hatton, "Toward Solvent-Free Continuous-Flow Electrochemically Mediated Carbon Capture with High-Concentration Liquid Quinone Chemistry", *Joule* **6**, 221 (2022). <https://doi.org/10.1016/j.joule.2021.12.001>
- [<sup>21</sup>] X. Li, X. Zhao, Y. Liu, T.A. Hatton, and Y. Liu, "Redox-Tunable Lewis Bases for Electrochemical Carbon Dioxide Capture", *Nature Energy* **7**, 1065 (2022). <https://doi.org/10.1038/s41560-022-01137-z>
- [<sup>22</sup>] M. Abdinejad, H. Seo, M.E. Lev Massen-Hane, and T.A. Hatton, "Oxygen-Stable Electrochemical CO<sub>2</sub> Capture Using Redox-Active Heterocyclic Benzodithiophene Quinone", *Angew. Chem. Int. Ed. Engl.* e202412229 (2024). <https://doi.org/10.1002/anie.202412229>
- [<sup>23</sup>] A. Liu, C.B. Musgrave, X. Li, W.A. Goddard, and Y. Liu, "Non-Aqueous Alkoxide-Mediated Electrochemical Carbon Capture", *Nature Energy* (2024). <https://doi.org/10.1038/s41560-024-01614-7>

- [<sup>24</sup>] X. Li, C. Deng, R. Chen, X. Li, F. Xie, Z. Wu, Y. Xie, S. Wang, and G.-M. Weng, "Exploiting Thiolate/Disulfide Redox Couples toward Large-Scale Electrochemical Carbon Dioxide Capture and Release", *Energy & Environmental Science* (2025). <https://doi.org/10.1039/d4ee04739g>
- [<sup>25</sup>] J. Liu, M. Yang, X. Zhou, and Z. Meng, "Solid-State Electrochemical Carbon Dioxide Capture by Conductive Metal-Organic Framework Incorporating Nickel Bis(Diimine) Units", *J. Am. Chem. Soc.* **146**, 33093 (2024). <https://doi.org/10.1021/jacs.4c10654>
- [<sup>26</sup>] R.J. Spreitzer and M.E. Salvucci, "Rubisco: Structure, Regulatory Interactions, and Possibilities for a Better Enzyme", *Annu. Rev. Plant Biol.* **53**, 449 (2002). <https://doi.org/10.1146/annurev.arplant.53.100301.135233>
- [<sup>27</sup>] G.J. Richards, J.P. Hill, N.K. Subbaiyan, F. D'Souza, P.A. Karr, M.R. Elsegood, S.J. Teat, T. Mori, and K. Ariga, "Pyrazinacenes: Aza Analogues of Acenes", *J. Org. Chem.* **74**, 8914 (2009). <https://doi.org/10.1021/jo901832n>
- [<sup>28</sup>] G.J. Richards and J.P. Hill, "The Pyrazinacenes", *Acc. Chem. Res.* **54**, 3228 (2021). <https://doi.org/10.1021/acs.accounts.1c00315>
- [<sup>29</sup>] K. Hatakeyama-Sato, T. Akahane, C. Go, T. Kaseyama, T. Yoshimoto, and K. Oyaizu, "Ultrafast Charge/Discharge by a 99.9% Conventional Lithium Iron Phosphate Electrode Containing 0.1% Redox-Active Fluoflavin Polymer", *ACS Energy Letters* **5**, 1712 (2020). <https://doi.org/10.1021/acsenergylett.0c00622>
- [<sup>30</sup>] D. Du, J. Zhou, Z. Yin, G. Feng, W. Ji, H. Huang, and S. Pang, "High-Voltage Recyclable Organic Cathode Enabled by Heteroatomic Substitution for Aqueous Zinc-Ion Batteries", *Advanced Energy Materials* **14**, (2024). <https://doi.org/10.1002/aenm.202400580>
- [<sup>31</sup>] D. Miklik, S. Fatemeh Mousavi, Z. Buresova, A. Middleton, Y. Matsushita, J. Labuta, A. Ahsan, L. Buimaga-Iarinca, P.A. Karr, F. Bures, G.J. Richards, P. Svec, T. Mori, K. Ariga, Y. Wakayama, C. Morari, F. D'Souza, T.A. Jung, and J.P. Hill, "Pyrazinacenes Exhibit on-Surface Oxidation-State-Dependent Conformational and Self-Assembly Behaviours", *Commun. Chem.* **4**, 29 (2021). <https://doi.org/10.1038/s42004-021-00470-w>
- [<sup>32</sup>] K. Amini, T. Cochard, Y. Jing, J.D. Sosa, D. Xi, M. Alberts, M.S. Emanuel, E.F. Kerr, R.G. Gordon, and M.J. Aziz, "In Situ Techniques for Aqueous Quinone-Mediated Electrochemical Carbon Capture and Release", *Nature Chemical Engineering* **1**, 774 (2024). <https://doi.org/10.1038/s44286-024-00153-y>
- [<sup>33</sup>] L.J. Murphy, K.N. Robertson, R.A. Kemp, H.M. Tuononen, and J.A.C. Clyburne, "Structurally Simple Complexes of CO<sub>2</sub>", *Chemical Communications* **51**, 3942 (2015). <https://doi.org/10.1039/C4CC08510H>
- [<sup>34</sup>] F.-Y. Kuo, S.E. Jerng, and B.M. Gallant, "Dual Salt Cation-Swing Process for Electrochemical CO<sub>2</sub> Separation", *ACS Central Science* **9**, 1750 (2023). <https://doi.org/10.1021/acscentsci.3c00692>
- [<sup>35</sup>] Y. Jing, E.W. Zhao, M.A. Goulet, M. Bahari, E.M. Fell, S. Jin, A. Davoodi, E. Jonsson, M. Wu, C.P. Grey, R.G. Gordon, and M.J. Aziz, "In Situ Electrochemical Recomposition of Decomposed Redox-Active Species in Aqueous Organic Flow Batteries", *Nat. Chem.* **14**, 1103 (2022). <https://doi.org/10.1038/s41557-022-00967-4>

## Methods

### Synthesis of FFDS

Fluoflavine (51 mmol, 11.9 g) was added into 95% H<sub>2</sub>SO<sub>4</sub> to afford a 0.5 M fluoflavine solution. The reaction mixture was stirred at 150 °C for 18 hours. After cooling down, the acid solution was slowly added into a 300 mL of ice water mixture. The resulting precipitate was then vacuum-filtered and washed with ice water to remove residual H<sub>2</sub>SO<sub>4</sub>. The product was then dried in vacuo at 60 °C overnight to afford the desired yellow product, fluoflavine disulfonic acid (**FFDS**), with a yield of 94%.

### Electrochemical Analysis

Cyclic voltammetry (CV) measurements were carried out with a CHI1140D electrochemical workstation. The three-electrode system includes a glassy carbon as the working electrode, a platinum wire as the counter electrode, and an Ag/AgCl (3 M KCl) as the reference electrode.

### Fourier-Transform Infrared (FTIR) Spectra

*In situ* Fourier transform infrared spectra were collected using an attenuated total reflectance infrared spectroscopy (ATR-IR) instrument from Bruker Tensor<sup>11</sup>. Spectra were collected on the neat samples at room temperature (around 25 °C). Spectra were plotted in transmittance (%) against the wavenumbers ( $\text{cm}^{-1}$ ).

### Fluorescence Emission Spectra

The fluorescence emissions of **FFDS** with different SOCs were measured with PerkinElmer FL-6500 fluorescence spectrometer. The source power is 40 kW and the frequency is 50 Hz. 255 nm was selected as excitation wavelength with 2.5 nm excitation slit width and a scan rate of 240 nm  $\text{min}^{-1}$ . 2.5 nm emission slit width, 320 nm emission filter, and 240 nm  $\text{min}^{-1}$  scan rate were selected as emission settings. The emission wavelength range was from 350 to 700 nm. 400 V was used as the photomultiplier voltage for acquisition.

### UV–Vis Absorption

The UV–Vis spectra of **FFDS** at different states of charge (SOCs) were collected from Shimadzu UV-1900 UV–Vis spectrometer.

### Flow cell setup

Flow cell experiments were constructed with the cell hardware from Fuel Cell Tech. The two electrolytes are separated with a cation exchange membrane Nafion 117. The electrodes were 5 pieces of baked carbon cloth on each side. Electrolytes were circulated by a peristaltic pump. A Lei-ci pH electrode (E-301-QC) was implemented for monitoring the electrolyte pH. The mass flow controller was a MFC-4200 (Siargo, Ltd.). CO<sub>2</sub> data was recorded with 100% CO<sub>2</sub> Sensor (SprintIR®-W CM-0221), 5% CO<sub>2</sub> Sensor (ExplorIR®-W CM-0124) and 1% CO<sub>2</sub> Sensor (K30 CM-0024). O<sub>2</sub> data was recorded by 25% Oxygen Flow Through Sensor (LOX-O<sub>2</sub>-F UV Flux CM-42991). The downstream CO<sub>2</sub> reading (ppm) is monitored with CO<sub>2</sub> sensors and recorded with the GasLab data logging software. All electrochemical characterizations were conducted and recorded on a BioLogic VMP-300 instrument.

### FFDS-based carbon capture and release in a simulated flue gas

The flow cell was galvanostatically charged and discharged at constant current densities followed with potential holds until current density decreased to 2 mA  $\text{cm}^{-2}$ . The charge process was followed by a 180-minute rest to complete CO<sub>2</sub> capture. The discharge process was followed by a 90-minute rest to complete CO<sub>2</sub> release. The simulated flue gas composed of 10% CO<sub>2</sub>, 10% O<sub>2</sub>, and 80% N<sub>2</sub> was used as the feed gas. The total pressure of the feed gas was one bar, and the flow rate was 30 mL  $\text{min}^{-1}$ . Before being fed into the **FFDS** negolyte, the feed gas was first flowed through a deionized water reservoir to be humidified to minimize the gas flow induced water loss over experiments. To avoid the influence of humidity on the accuracy of sensor readings, a drying tube filled with blue silica gel (Chemicon, 6–20 mesh) was installed before the downstream gas entered the gas sensors. CO<sub>2</sub> data was recorded by a 100% CO<sub>2</sub> sensor. O<sub>2</sub> data was recorded by a 25% O<sub>2</sub> sensor.

### FFDS sorbent-based three-day indoor/outdoor DAC, CO<sub>2</sub> release, and regeneration

The 100% SOC **FFDS** sorbent was transferred to a 50 mL PTFE beaker equipped with a cylindrical stir bar and being stirred in ambient air at a speed of 500 rpm for the three-day direct air capture (DAC), both indoors and outdoors. After the three-day DAC, approximately 5–7 mL of water was added to compensate for the evaporation-induced water losses. The pH of the **FFDS** sorbent decreased from the initial 13.3 to ~10.2 after DAC. The CO<sub>2</sub>-captured **FFDS** sorbent was then transferred back to the negolyte reservoir, and the flow cell was reconnected for discharge-induced CO<sub>2</sub> release. Pure N<sub>2</sub> served as the carrier gas at a flow rate of 28 mL  $\text{min}^{-1}$ . To minimize the evaporation-induced water losses in the negolyte during the electrochemical measurements, N<sub>2</sub> was humidified by flowing the gas through a deionized water reservoir before being introduced to the **FFDS** negolyte. The N<sub>2</sub> gas outlet was positioned at the bottom of the **FFDS** negolyte to ensure that all of the released CO<sub>2</sub> during the discharge can be bubbled out from the negolyte and being detected by the CO<sub>2</sub> sensor. To better measure the volume of the released CO<sub>2</sub>, the CO<sub>2</sub> flow rates before and after CO<sub>2</sub> release should be approximated to 0 mL  $\text{min}^{-1}$  to generate a baseline. We let N<sub>2</sub> flow through the CO<sub>2</sub> sensors for a while before initiating the CO<sub>2</sub> release and after the completion of the CO<sub>2</sub> release.

The flow cell was discharged at 20 mA  $\text{cm}^{-2}$  followed by potential holds. −0.5 V was applied for **normal discharge** until the current density decreased to 2 mA  $\text{cm}^{-2}$ . −1.2 V was applied for **deep discharge**

until the pH of negolyte decreased to 4. The CO<sub>2</sub> release process was considered complete when the 5% CO<sub>2</sub> sensor reading stabilized at ~200 ppm.

After the completion of CO<sub>2</sub> release, the flow cell was charged in N<sub>2</sub> to regenerate the **FFDS** sorbent at 20 mA cm<sup>-2</sup> followed by a potential hold at 1.0 V until the current density decreased to 2 mA cm<sup>-2</sup>.

#### **FFDS sorbent-based accelerated overnight DAC, CO<sub>2</sub> release, and regeneration**

Powered by an electric air pump, the ambient air was pumped through a deionized water reservoir to be humidified, before being introduced into the **FFDS** sorbent through a PTFE tube (Ø3.2 mm). As such, the water loss induced by the rapid gas flow can be significantly minimized. The air outlet was positioned at the bottom of the **FFDS** sorbent to increase the air-liquid interface for sufficient CO<sub>2</sub> capture. The air flow rate was regulated at 375 mL min<sup>-1</sup> with a mass flow controller (Siargo, Ltd. MFC-4200). With such a high flow rate, the whole DAC process was greatly accelerated. The pH of the **FFDS** sorbent decreased from 13.3 to around 10.0 after the overnight air bubbling. To avoid the influence of humidity on the accuracy of sensor readings, a drying tube filled with blue silica gel was installed before the downstream gas entered the gas sensors. The CO<sub>2</sub> reading during the accelerated overnight DAC was recorded with the 1% CO<sub>2</sub> sensor. After the accelerated overnight DAC, the air was replaced by N<sub>2</sub> at a flow rate of 28 mL min<sup>-1</sup>. Serving as the carrier gas, N<sub>2</sub> flowed through the **FFDS** negolyte for 30 minutes to generate a baseline of CO<sub>2</sub> level at ~200 ppm before discharge process. The flow cell was discharged at 20 mA cm<sup>-2</sup> until the voltage approached the pre-set cutoffs. A potential hold at -0.5 V was applied for normal discharge until the current density decreased to 2 mA cm<sup>-2</sup>. A potential hold at -1.2 V was applied for deep discharge until the pH of the negolyte dropped to 4. The CO<sub>2</sub> release was considered complete when the CO<sub>2</sub> sensor reading stabilized at ~200 ppm.

The flow cell was charged in N<sub>2</sub> to regenerate the **FFDS** sorbent at 20 mA cm<sup>-2</sup> followed by a potential hold at 1.0 V until the current density decreased to 2 mA cm<sup>-2</sup>.

#### **Data and material availability**

All experimental data are available in the main text or Supplementary Information. Source data are provided in this paper.

#### **Acknowledgments**

Research at National University of Singapore was supported by the Presidential Young Professorship startup grant. Research at University of Science and Technology of China was supported by the National Science Foundation of China (22305238, 22475203). Research at Beijing University of Posts and Telecommunications was supported by the National Natural Science Foundation of China (22203009).

#### **Author contributions**

Y.J., Z.M., Y.L. supervised the project. Y.J. conceived the idea. Y.J., Z.M., and Y.L. designed the experiment. Z.W. and J.L. performed the synthesis and characterization. Z.W., J.L., M.T. and A.L. performed spectroscopic studies. S.X. performed the electrochemical CO<sub>2</sub> capture from simulated flue gas and DAC tests. S.X. and K.Z. performed three-electrode measurement. X.W. calculated the DIC over DAC. K.T. optimized the gas sensor setup and the data collection. All authors contributed to the discussion of the project. Y.J. and S.X. wrote the manuscript with input from all co-authors.

#### **Competing interests**

The National University of Singapore has applied for a patent on the material and technology discussed herein regarding electrochemically induced carbon capture from flue gas or air with **FFDS** sorbent via its technology transfer innovation office on which Y.J., Z.W., and S.X. are listed as co-inventors (application no. 10202500648U).